Supplementary Materials for:

Evofosfamide for the treatment of human papillomavirus-negative head and neck squamous cell carcinoma

Stephen M.F. Jamieson[1,2,3], Peter Tsai[4], Maria K. Kondratyev[5], Pratha Budhani[6], Arthur Liu[6], Neil N. Senzer[7], E. Gabriela Chiorean[8,9], Shadia I. Jalal[8], John J. Nemunaitis[10], Dennis Kee[11], Avik Shome[1], Way W. Wong[1], Dan Li[1], Nooriyah Poonawala-Lohani[12], Purvi M. Kakadia[4], Nicholas S. Knowlton[4], Courtney R.H. Lynch[1], Cho R. Hong[1], Tet Woo Lee[1,2], Reidar A. Grénman[13], Laura Caporiccio[5], Trevor D. McKee[14], Mark Zaidi[3,14], Sehrish Butt[14], Andrew M.J. Macann[15], Nicholas P. McIvor[16], John M. Chaplin[16], Kevin O. Hicks[1,2], Stefan K. Bohlander[2,4], Bradly G. Wouters[5,17,18], Charles P. Hart[19], Cristin G. Print[2,4], William R. Wilson[1,2], Michael A. Curran[6], Francis W. Hunter[1,2*]

[1]Auckland Cancer Society Research Centre, University of Auckland, Auckland, New Zealand;
[2]Maurice Wilkins Centre for Molecular Biodiscovery, University of Auckland, Auckland, New Zealand;
[3]Department of Pharmacology and Clinical Pharmacology, University of Auckland, Auckland, New Zealand;
[4]Department of Molecular Medicine and Pathology, University of Auckland, Auckland, New Zealand;
[5]Princess Margaret Cancer Centre, University Health Network, Toronto, ON, Canada;
[6]Department of Immunology, University of Texas, MD Anderson Cancer Center, Houston, TX;
[7]Mary Crowley Cancer Research Center, Dallas, TX;
[8]Indiana University Melvin and Bren Simon Cancer Center, Indiana University, Indianapolis, IN;
[9]Fred Hutchinson Cancer Research Center, University of Washington, Seattle, WA;
[10]Department of Medicine, University of Toledo College of Medicine and Life Sciences, University of Toledo, Toledo, OH;
[11]LabPLUS, Auckland City Hospital, Auckland, New Zealand;
[12]The Bioinformatics Institute, School of Biological Sciences, University of Auckland, Auckland, New Zealand;
[13]Department of Otolaryngology–Head and Neck Surgery, Turku University Hospital, Turku, Finland;
[14]STTARR Innovation Centre, University Health Network, Toronto, ON, Canada,
[15]Department of Radiation Oncology, Auckland City Hospital, Auckland, New Zealand;
[16]Department of Otolaryngology–Head and Neck Surgery, Auckland City Hospital, Auckland, New Zealand;
[17]Department of Radiation Oncology, University of Toronto, Toronto, ON, Canada;
[18]Department of Medical Biophysics, University of Toronto, Toronto, ON, Canada;
[19]Threshold Pharmaceuticals, South San Francisco, CA.

**Corresponding author email: f.hunter@auckland.ac.nz*

Table of Contents

Contents of Supplementary Data File

Tab	Description
1	Mutations (SNVs and indels) detected in 22 HNSCC cell lines by whole-exome sequencing
2	IC_{50} data for evofosfamide, Br-IPM, SN30000, PR-104A, cisplatin and 5-FU in HNSCC cell lines under anoxia and ambient air
3	Differentially expressed genes (log_2-transformed FPKM) in evofosfamide-sensitive and evofosfamide-resistance HNSCC cell lines
4	Expression values (log_2-transformed FPKM) for the proliferation metagene in HNSCC cell lines

1. Supplementary Methods

1.1 Determination of Ploidy in HNSCC Cell Lines

Log-phase cultures were trypsinized and 10^6 cells in suspension were pelleted by centrifugation. The supernatant was removed and the cells were fixed by the dropwise addition of 1 mL cold 70% ethanol and incubated at 4°C for ≥30 min. The cells were re-pelleted and the ethanol was replaced with 1 mL PBS containing 3% FBS. This was repeated twice to rinse the cells. RNAse (100 µg/mL; Roche 10109134001) and propidium iodide (20 µg/mL; Sigma–Aldrich P-4170) were added and the cells were incubated for 10 min in the dark at room temperature. Flow cytometry was performed with a BD Accuri C6 flow cytometer using a 488 nm laser for excitation and fluorescence emission detected using a 585/40 filter. The data were analyzed using ModFit LT v4.1.7 (Verity Software House). The ploidy of the cells was approximated by measuring their relative DNA content, defined as the fluorescence of the G0/G1 peak for cell singlets relative to half of that for a HCT 116 diploid control (i.e. HCT 116 DNA content defined as 2.0). HCT 116 was obtained from ATCC (Manassas, VA).

1.2 Whole-Genome CRISPR Knockout Screens

UT-SCC-74B cells were stably transduced with *Streptococcus pyogenes* Cas9 (lentiCas9-Blast vector) at a multiplicity of infection (MOI) of 0.25 and expression confirmed by immunoblotting (mouse anti-Cas9 monoclonal antibody 7A9; Diagenode; Liege, Belgium). The resulting pool was transduced with the GeCKOv2 sgRNA library (3) (lentiGuide-Puro vector) at an MOI of 0.2 and a scale of 140 transductants per sgRNA. After 7 d selection in puromycin, separate pharmacological selections with evofosfamide and Br-IPM were initiated from this founder library, each in duplicates of 10^8 cells, with untreated duplicate control cultures of $\geq 3 \times 10^7$ cells maintained in continuous culture for each drug until endpoint. Cultures were exposed to 0.8 µM evofosfamide for 1 h under anoxia as stirred suspensions in an anaerobic chamber as above, at 0.5×10^6 cells per mL, with 30-min drug-free pre-incubation to deplete residual oxygen. Thereafter, drug was removed and cells plated under ambient oxygen for recovery. Selection with 130 µM Br-IPM was imposed on log-phase monolayer cultures as continuous exposure without drug replacement. Recovered cultures were harvested for analysis 16 and 20 d after selection with evofosfamide and Br-IPM, respectively. A pilot-scale functional validation screen used a library of 4×10^7 transductants exposed to 3 µM 6-thioguanine prior to recovery. Genomic DNA was isolated using a QIAamp DNA Blood Maxi Kit (Qiagen) and sgRNA sequences PCR-amplified for sequencing as described (3, 4). Sequencing was performed on a NextSeq500 (Illumina) using a high-output, 150 bp paired-end flow cell and 5% PhiX. Reads were trimmed at the 5'- and 3'-ends using Cutadapt and trimmed reads that contained base call failures or had lengths other than 20 bp excluded using Awk scripts. Reads were then aligned to the GeCKOv2 index using BWA, sorted using SAMtools and read counts scored and quality and distribution outputs generated in R. Statistical significance of positive and negative selection of sgRNAs in treated relative to control cultures was assessed using the RIGER (5) algorithm with weighted sum aggregation.

1.3 Targeted DNA sequencing of PDX models

DNA was extracted from the clinical tumor specimens and second-generation PDX models using the Qiagen DNeasy Blood & Tissue kit. DNA quality was determined by the ratio of absorbance at 260 nm to 280 nm (≥1.8) and at 260 nm to 230 nm (≥1.5) on a NanoDrop ND-1000 spectrophotometer (Thermo Fisher Scientific), with quantitation on a Qubit 3.0 fluorometer (Thermo Fisher Scientific). Ethanol precipitation was utilized to enhance DNA quality if required. DNA (200 ng per sample) was resolved on a 0.8% agarose/0.5% Tris-borate-EDTA gel to assess degradation. DNA libraries for sequencing of 409 genes using the Ion AmpliSeq Comprehensive Cancer Panel

(Thermo Fisher Scientific) were prepared using Ion AmpliSeq Library Kit 2.0 (Thermo Fisher Scientific), whereby targeted loci were amplified by PCR (GeneAmp PCR system 9700, Thermo Fisher Scientific), followed by digestion of primer sequences and ligation of Ion Xpress barcode adaptors (Thermo Fisher Scientific) to the amplicons. The barcoded libraries were purified using the Agencourt AMPure XP kit (Beckman Coulter; Brea, CA) and were quantified by qRT-PCR (QuantStudio 6 Flex real-time PCR system, Thermo Fisher Scientific) using the Ion Library TaqMan Quantitation kit (Thermo Fisher Scientific). DNA libraries were sequenced on an Ion Proton (Thermo Fisher Scientific) and the reads were mapped and variants called using Ion Reporter 5.4 (Thermo Fisher Scientific). Driver mutations were defined as variants with minor allele frequencies <0.001 in ExAC, P-values <0.001, confirmed pathogenic somatic mutations in COSMIC v82 and called in ≥1 HNSCC sample on cBioPortal.

1.4 Pimonidazole Immunostaining of PDX and CDX Tumors

For analysis of hypoxic fraction, tumor-bearing mice were administered 60 mg.kg-1 pimonidazole in saline by i.p. injection and culled 2 h thereafter for staining. Excised tumors were fixed in 10% neutral-buffered formalin for 24-48 h. The tissue was then stored in 70% histology ethanol until paraffin-embedding and sectioning. Sections on glass slides were deparaffinized and rehydrated by heating to 58°C for 60 min, followed by rinsing in xylene, ethanol and water. The sections were placed in 10 mM citrate buffer, pH 6.0 and heated in a pressure cooker for antigen retrieval, and then rinsed with Tris-buffered saline (TBS) followed by TBS containing 0.1% Tween-20 (TBST). Sections were blocked with 10% goat serum in TBST at 4°C for 1 h and then incubated in pimonidazole-FITC (mouse monoclonal antibody 4.3.11.3 diluted 1:50 in blocking buffer; NPI Inc) overnight at 4°C. Sections were rinsed in TBST and the nuclei were stained with H33258 (Thermo Fisher Scientific). After rinsing in TBS, slides were mounted with coverslips and sealed. Images of the whole tissue section were acquired using an Axio Imager 2 microscope (Zeiss) with a Vslide scanner (MetaSystems). Images were analyzed using ImageJ (v1.51) to determine the area within the section that was pimonidazole-positive (hypoxic) as a fraction of the total area after excluding necrotic regions. Tumor necrosis was identified as the absence of H33258 staining and was confirmed by histopathological examination of H&E stained sections.

1.5 CA9 and *Pan*-Cytokeratin Immunohistochemistry, Imaging and Quantitation in Tumor Sections

Six days after completing treatment with evofosfamide monotherapy or in combination with image-guided cervical lymph node irradiation (see Methods), mice bearing spontaneously disseminated UT-SCC-74B tumors were administered 1 mg i.v. H33258 (Sigma-Aldrich) and sacrificed 1 min thereafter by isofluorane overdose. Tumor-bearing nodes were dissected, flash-frozen and embedded in OCT. Sections were cut at 5 μm, mounted onto slides and air-dried for 30 min. The sections were fixed in 2% paraformaldehyde, permeabilized with PBS-T + 0.5% Triton X-100 and stained with anti-CA9 polyclonal antibody (NB100-417SS, R&D Systems; Minneapolis, MN) diluted 1:50 or anti-cytokeratin monoclonal antibody (AE1/AE3, Dako; Glostrup, Denmark) diluted 1:500 overnight at 4°C. After staining with secondary antibodies, tissue was imaged on a TissueScope slide scanner (Huron Digital Pathology; Waterloo, ON) to identify regions of H33258-positive perfused regions. Immunostaining was performed on serial tissue sections for CA9 plus DAPI or pan-cytokeratin (AE1/AE3) plus DAPI, and slides were digitized on an Axio Scan whole- fluorescence slide scanner (Zeiss; Oberkochen, Germany). These serial fluorescence images were then aligned manually using a custom MATLAB script and aligned images were imported into Definiens TissueStudio software (v4.2; Munich, Germany) for analysis. Regions containing tissue were segmented into ‘tumor’, ‘necrosis’, ‘normal tissue’ and ‘folds/artifacts’ by semi-automated machine-learning segmentation with manual correction, utilizing pan-cytokeratin staining and nuclear morphology to discriminate tumor from normal tissue and absence of nuclear staining and morphology to identify necrosis. Nuclear segmentation was then performed to identify individual

cells based on a DAPI threshold, and cells were simulated by growing out from nuclei by up to 3 μm. Mean CA9-staining intensity was measured on a per-cell basis and cells were classified into negative, low, medium and high for CA9 and the proportion in each class was exported for the tumor region.

2. Supplementary Figures

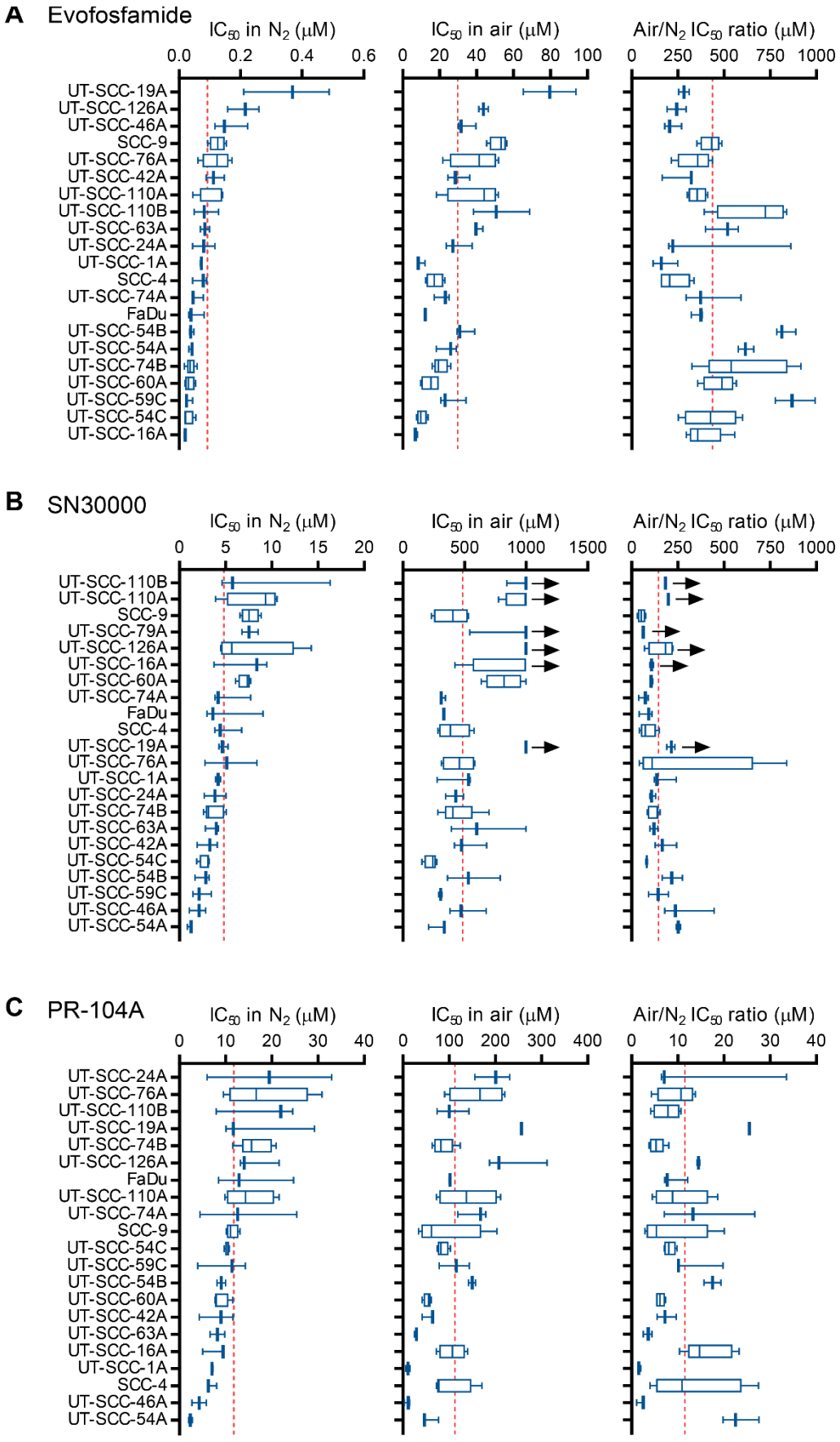

Figure S1 (preceding page). Antiproliferative potency and hypoxic selectivity of evofosfamide **(A)**, SN30000 **(B)** and PR-104A **(C)** against cultured head and neck squamous cell carcinoma (HNSCC) cell lines. Antiproliferative activity was assessed by IC_{50} assay (determining the drug concentration for 50% inhibition of cell growth) under anoxia (N_2) or ambient oxygen (air), with hypoxic selectivity represented as the Air-N_2 IC_{50} quotient. Boxes denote the median and interquartile range, while whiskers mark the minimum and maximum from ≥3 independent determinations. The Air-N_2 ratio is derived from ≥3 intra-experiment quotients calculated from anoxic and normoxic assays performed on the same days. Dashed lines denote the mean IC_{50} values for the cell line panel. Black arrows denote IC_{50} values that were beyond upper the range of the assay.

Figure S2 (next page). Antiproliferative potency and hypoxic selectivity of Br-IPM **(A)** and the standard chemotherapeutic agents cisplatin **(B)** and 5-fluorouracil (5-FU) **(C)** against cultured head and neck squamous cell carcinoma (HNSCC) cell lines. Antiproliferative activity was assessed by IC_{50} assay (determining the drug concentration for 50% inhibition of cell growth) under anoxia (N_2) or ambient oxygen (air), with hypoxic selectivity represented as the Air-N_2 IC_{50} quotient. Boxes denote the median and interquartile range, while whiskers mark the minimum and maximum from ≥3 independent determinations. The Air-N_2 ratio is derived from ≥3 intra-experiment quotients calculated from anoxic and normoxic assays performed on the same days. Dashed lines denote the mean IC_{50} values for the cell line panel.

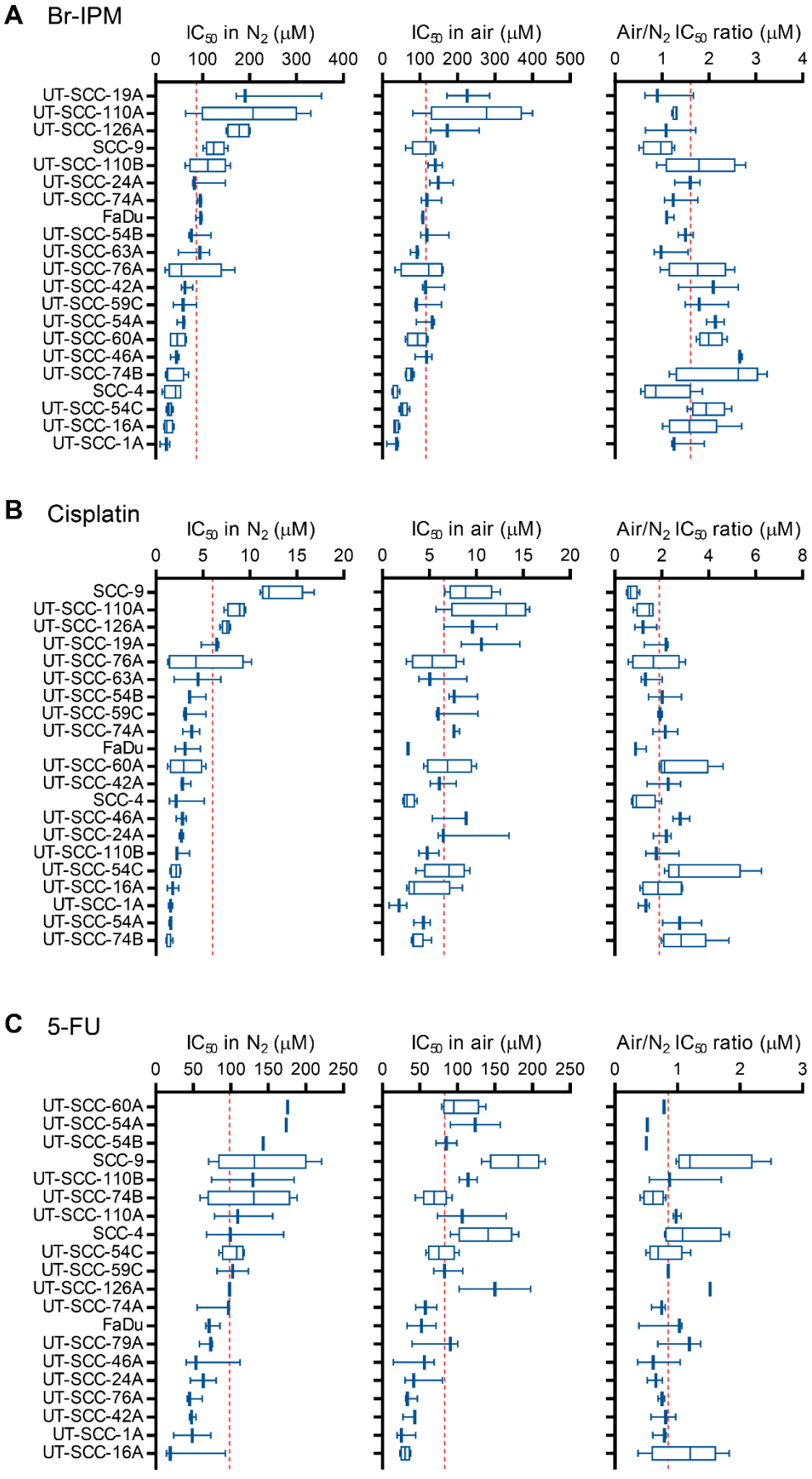
A
Br-IPM
IC50 in N2 (μM)
0 100 200 300 400
IC50 in air (μM)
0 100 200 300 400 500
Air/N2 IC50 ratio (μM)
0 1 2 3 4
UT-SCC-19A
UT-SCC-110A
UT-SCC-126A
SCC-9
UT-SCC-110B
UT-SCC-24A
UT-SCC-74A
FaDu
UT-SCC-54B
UT-SCC-63A
UT-SCC-76A
UT-SCC-42A
UT-SCC-59C
UT-SCC-54A
UT-SCC-60A
UT-SCC-46A
UT-SCC-74B
SCC-4
UT-SCC-54C
UT-SCC-16A
UT-SCC-1A
B
Cisplatin
IC50 in N2 (μM)
0 5 10 15 20
IC50 in air (μM)
0 5 10 15 20
Air/N2 IC50 ratio (μM)
0 2 4 6 8
SCC-9
UT-SCC-110A
UT-SCC-126A
UT-SCC-19A
UT-SCC-76A
UT-SCC-63A
UT-SCC-54B
UT-SCC-59C
UT-SCC-74A
FaDu
UT-SCC-60A
UT-SCC-42A
SCC-4
UT-SCC-46A
UT-SCC-24A
UT-SCC-110B
UT-SCC-54C
UT-SCC-16A
UT-SCC-1A
UT-SCC-54A
UT-SCC-74B
C
5-FU
IC50 in N2 (μM)
0 50 100 150 200 250
IC50 in air (μM)
0 50 100 150 200 250
Air/N2 IC50 ratio (μM)
0 1 2 3
UT-SCC-60A
UT-SCC-54A
UT-SCC-54B
SCC-9
UT-SCC-110B
UT-SCC-74B
UT-SCC-110A
SCC-4
UT-SCC-54C
UT-SCC-59C
UT-SCC-126A
UT-SCC-74A
FaDu
UT-SCC-79A
UT-SCC-46A
UT-SCC-24A
UT-SCC-76A
UT-SCC-42A
UT-SCC-1A
UT-SCC-16A

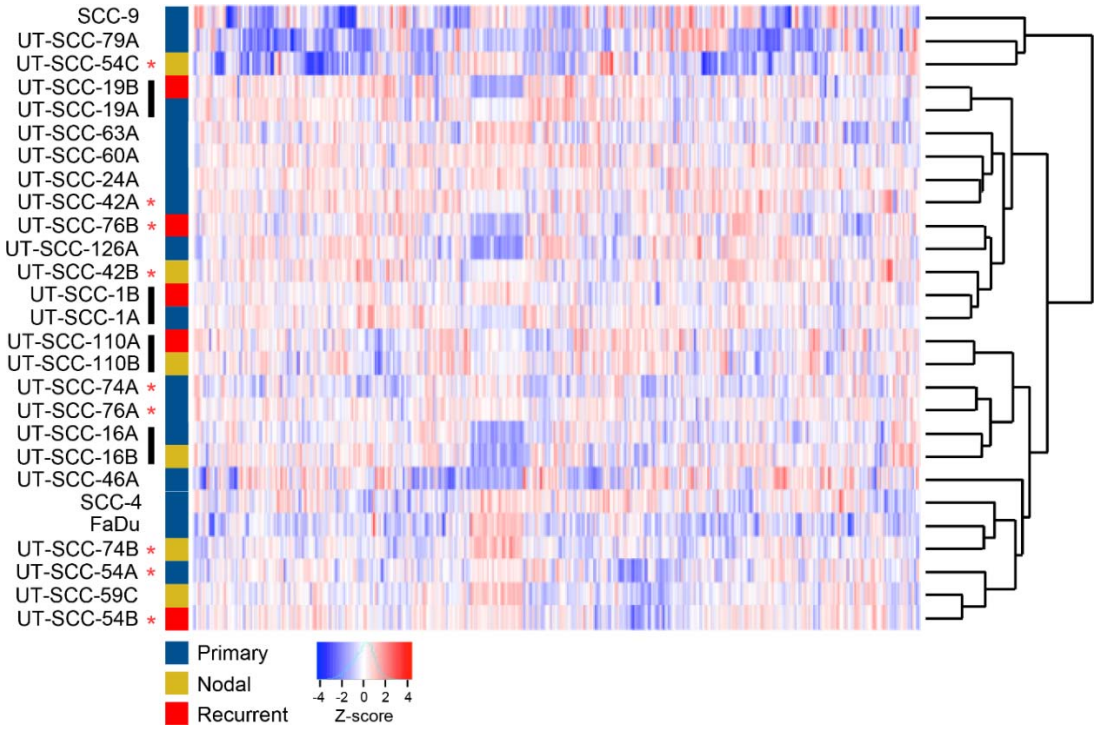

Figure S3. Comparison of gene expression profiles in head and neck squamous cell carcinoma (HNSCC) cell lines. RNA sequencing was performed on cell lines cultured under ambient oxygen conditions. Unsupervised hierarchical clustering was performed in R using the ward.D method with Euclidean distance and clustered according to the 85th to 99th percentile of all transcripts with ≥10 mapped reads ranked for variance in expression. The positions of cell lines derived from primary, nodal or recurrent lesions are indicated. Black bars denote matched cell lines from individual patients that cluster together. Matched cell lines from individual patients that clustered distantly are marked with asterisks.

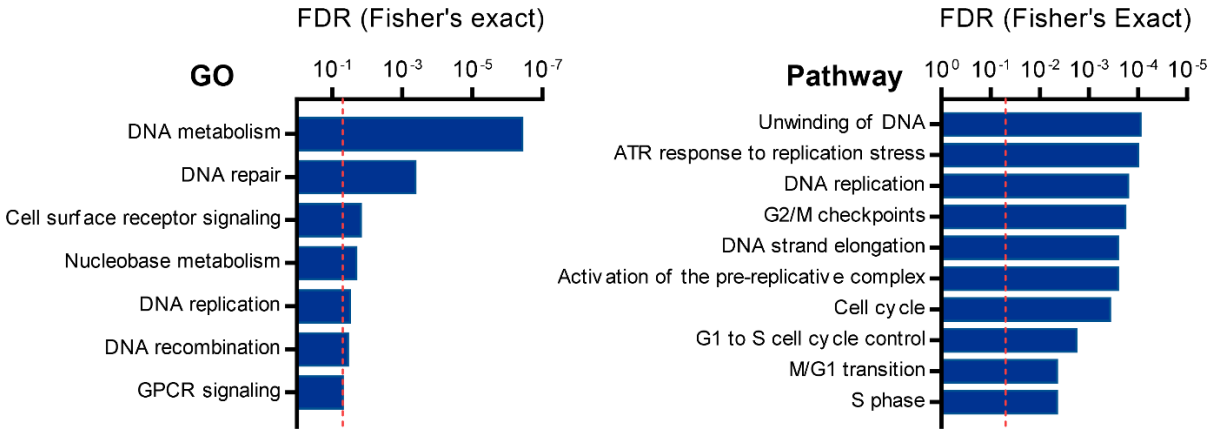

Figure S4. Enrichment of gene ontology (GO; left panel) and molecular pathway (right panel) terms among expressed genes (RNAseq) that correlated with sensitivity to evofosfamide (per IC_{50} assay under anoxia) in head and neck squamous cell carcinoma (HNSCC) cell lines. Correlations were computed using the Spearman method and the top 200 correlating genes were queried for the enrichment of GO and pathway terms using PANTHER (6) and GeneSetDB (7), respectively. Statistical significance was assessed by Fisher's exact test. False discovery rates (FDR) determined using Benjamini–Hochberg method are plotted, with dashed lines denoting 5% FDR.

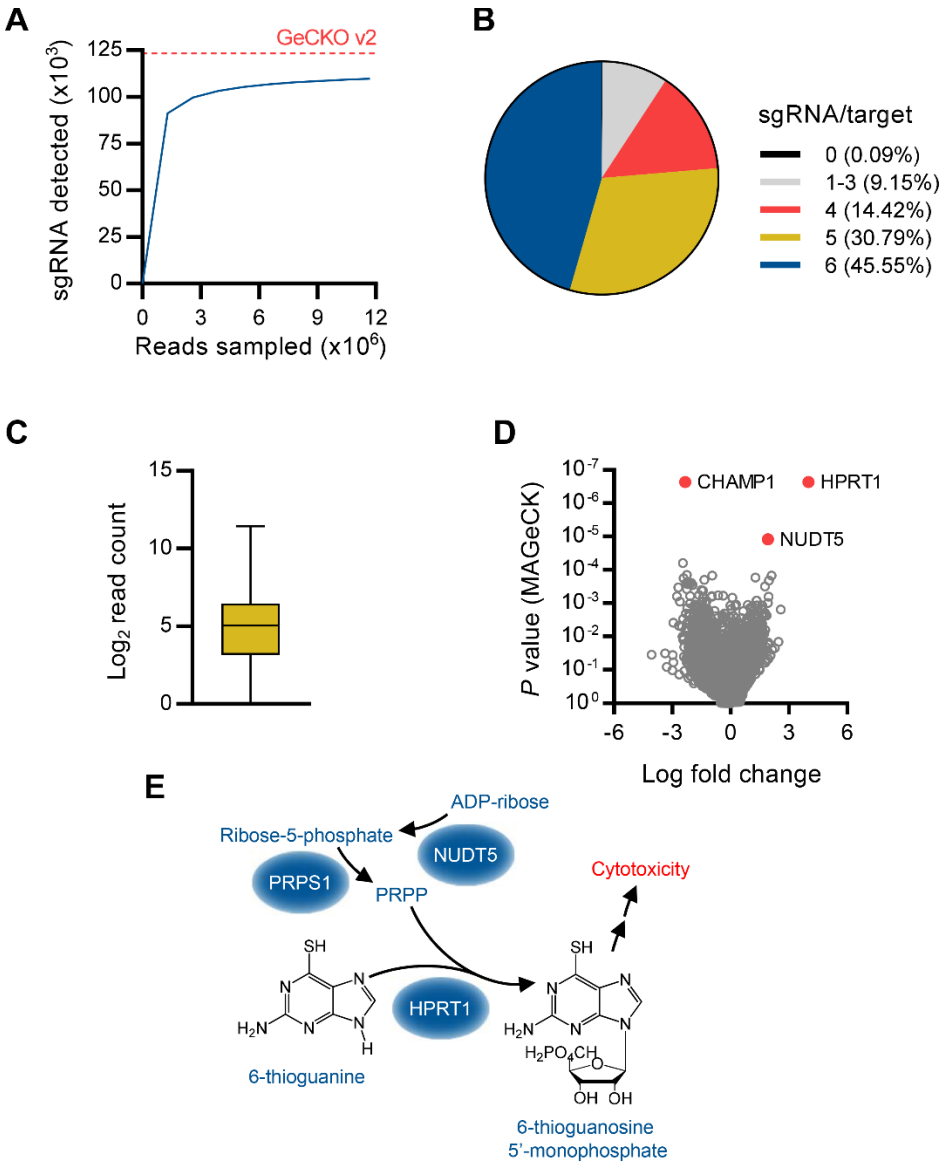

Figure S5. Characterization and functional validation of a genome-scale gene knockout library established in UT-SCC-74B using the GeCKOv2 sgRNA pool (3). **(A)** Characterization of library complexity by subsampling analysis of single guide RNA (sgRNA) sequencing reads. The number of unique sgRNA detected (≥1 mapped read) is plotted as a function of the size of random subsamples (rarefy function within the vegan *R* package) of next-generation sequencing reads. The total size of the human GeCKOv2 library (123,411 sgRNA) is denoted by the dashed line. **(B)** The proportion of sgRNA targets (i.e. genes and miRNA) represented by 0, 1-3, 4, 5 or 6 sgRNA in the UT-SCC-74B gene knockout library. Note that GeCKOv2 has a redundancy of 6 sgRNA per each of 19,050 gene targets and 4 sgRNA per each of 1,684 miRNA targets. **(C)** Distribution of $\log_2$-transformed read counts across all sgRNA in GeCKOv2 represented in a box-and-whisker plot, which denote the median, interquartile range and minimum and maximum. **(D)** Enrichment of UT-SCC-74B cells carrying sgRNA targeted to *HPRT1* and *NUDT5* in a functional validation screen using 6-thioguanine. In this pilot-scale screen, 10^7 cells were exposed to 3 µM 6-thioguanine for 4 d then 5 µM for 4 d further. The cultures then recovered for 13 d without treatment prior to sequencing. The volcano plot shows the statistical significance of gene-level enrichment or depletion (as assessed using the MAGeCK algorithm (8)) as a function of the median $\log_2$ fold change in normalized read counts of sgRNA against each target in treated relative to non-treated cultures. **(E)** Mechanism of activation of 6-thioguanine, highlighting the contributions of NUDT5 (9) and HPRT1 (10). The biological significance of positive selection for sgRNA targeting *CHAMP1*, a gene involved in chromosome alignment and segregation at mitotic metaphase (11), is unknown.

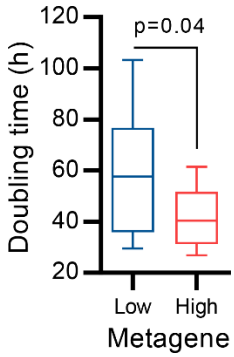

Figure S6. Doubling times of head and neck squamous cell carcinoma (HNSCC) cell lines classified proliferation^{low} (n=13) or proliferation^{high} (n=14) by hierarchical clustering of metagene expression values (Figure 3F). Population doubling times were estimated using 2-6 recordings of cell density following trypsinization of continuous log-phase monolayer cultures (with cell counts obtained using a Z series Coulter Counter, Beckman Coulter) and did not account for cell cycle delay following subculture. Boxes denote the median and interquartile range, while whiskers mark the minimum and maximum values. Statistical significance assessed by two-tailed Student's t-test.

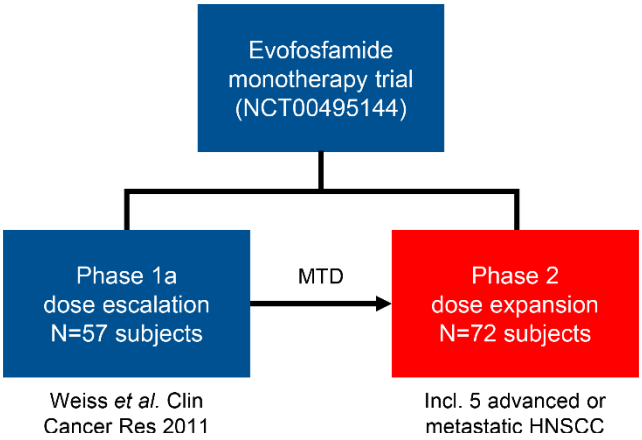

Figure S7. Phase 1a dose-escalation and phase 2 dose-expansion components of the NCT00495144 evofosfamide monotherapy trial in solid tumors.

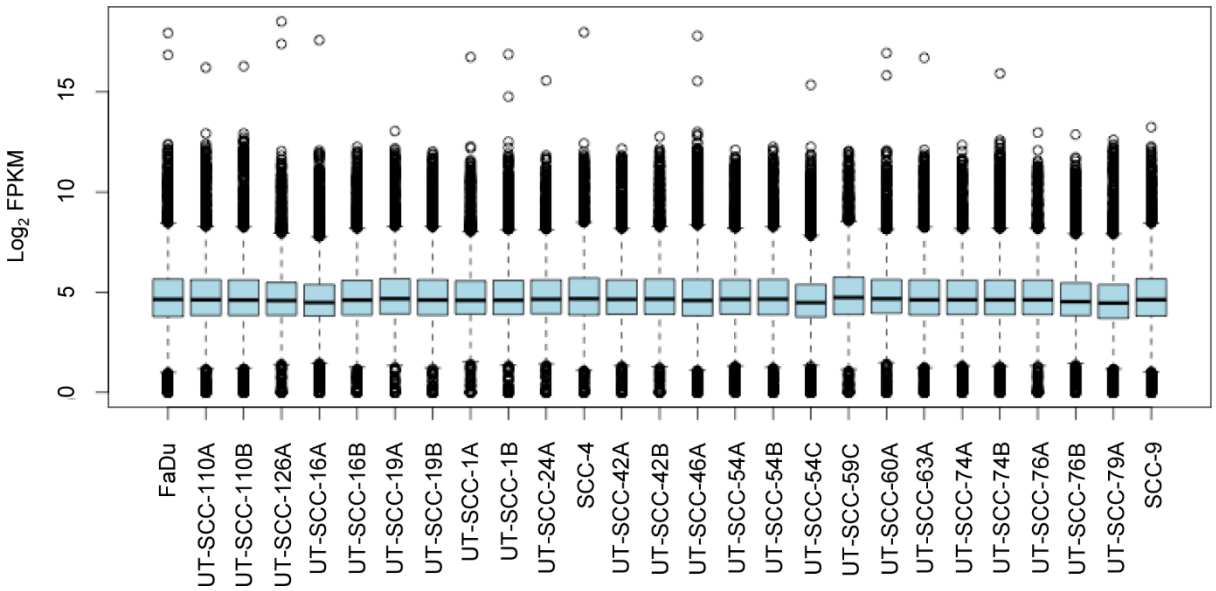

Figure S8. Distributions of gene expression values (as $\log_2$ Fragments Per Kilobase of transcript per Million mapped reads, FPKM) measured by RNA sequencing in head and neck squamous cell carcinoma (HNSCC) cell lines. Boxes show the median and interquartile range, while whiskers denote the 5th and 95th percentiles of $\log_2$-transformed FPKM counts for all annotated mRNA.

3. Supplementary Tables

Table S1. Multiple linear regressions of log Br-IPM IC_{50} and the log of the sum of the intracellular concentration of Br-IPM and Cl-IPM after 1 h exposure to evofosfamide at 30 µM (as measures of reductive evofosfamide activation) as predictors of evofosfamide IC_{50} under anoxia. VIF = variance inflation factor.

Predictors	**Coefficient**	**SEM**	**t**	**P**	**VIF**	**R**	**R^2**	**Adj. R^2**
Constant Br-IPM IC_{50} (µM)	-1.524 0.00321	0.114 0.0009	-13.391 3.532	<0.001 0.005	-	0.729	0.531	0.489
Constant Log Br-IPM (nM) + log Cl-IPM (nM)	-0.078 -0.482	0.675 0.282	-0.116 -1.706	0.910 0.116	- 1.000	0.457	0.209	0.137
Constant Br-IPM IC_{50} (µM) Log Br-IPM (nM) + log Cl-IPM (nM)	-1.383 0.736 -0.502	0.511 0.168 0.173	-2.709 4.378 -2.895	0.022 0.001 0.016	1.001 1.001	0.854	0.729	0.675

Table S2. Selected genomic variants identified in patient-derived xenograft (PDX) models. MAF = mutant allele frequency.

PDX model	**Gene**	**Variant**	**Function**	**MAF**
ACS-HN06	*TP53* *TET2* *KMT2C* *KMT2C* *KAT6B*	R248Q Y867H Y816term D348N E1097del	Missense Missense Nonsense Missense Deletion	1.00 1.00 0.42 0.30 0.82
ACS-HN07	*PIK3CA* *TP53*	E545K R342term	Missense Nonsense	0.20 0.11
ACS-HN08	*HRAS* *TP53* *NOTCH1* *XRCC2* *MET* *KMT2C* *KMT2C* *ASXL1*	G13V E339term C1536Y L117fs N375S Y816term D348N G1397S	Missense Nonsense Missense Deletion Missense Nonsense Missense Missense	0.98 0.29 1.00 0.86 1.00 0.23 0.10 0.54

Table S3. Short tandem repeat (STR) profiles for UT-SCC cell lines. Values in parentheses denote minor alleles.

Cell line	TH01	D3S135B	Vwa	D21S11	TPOX	D7S820	D19S433	D5S818	D2S1338	D16S539	CSF1PO	D13S317	FGA	D18S51	D8S1179	AMEL
UT-SCC-1A	9	18	15, 17	29, 31	8, 9	9	15	11, 12	25	11	10, 12	9, 10	22, 24	16	10, 11	X
UT-SCC-1B	9	14, 15	15, 17	29, 31	8, 9	8, 9	15	11, 12	25	11	10, 12	9, 10	22, 24	16	10, 11	X
UT-SCC-16A	8	16	17, (18, 19), 20	30.2	8	9, 10	13, 16	12	17, 25	9, 12	11	11, 12	20	12, 16	9, 13	X
UT-SCC-16B	7.9	14, 17	18, 19	31, 32.2	9	9, 11	14, 15.2	12, 14	27	11	10, 11	9, 12	21, 22	14, 15	12, 13	X
UT-SCC-19A	6	15	14, 19	30, 32.2	8, 10	12	13.2, 18.2	12	19	12, 13	12	11, 12, 13	24	16	10, 14	X
UT-SCC-19B	6	15	14, 19	32.2	8	12	18.2	10, 12	19	12	12	11, 13	24	16	10, 14	X
UT-SCC-24A	9.3	16	16, 18	29, 30	11	(8), 11	12, 14.2	10	19, 20	11	13	12, 14	19, 22	18	13, 15	X
UT-SCC-42A	9, 9.3	14	17, 18	28, 30	8	7, 10	14, 15.2	11	17, 26	11, 13	11, 13	8, 11	23	15	11, 13	X
UT-SCC-42B	9, 9.3	14	17, 18	28, 30	8	7, 10	14, 15.2	11	17, 26	11, 13	11, 13	8, 11	22. 2, 23	15	11, 13	XY
UT-SCC-46A	9, 9.3	16	16, 17, 18	29, 30	8	10, 12	(13), 14	11	20	11	10, 11	9, 14	22, 24	13, 15	14, 15	XY
UT-SCC-54A	9.3	17	14, 18	31, 32.2	8, 9	12, OL	14	11	20, 24	11, 12	10	12	26	14, 16	10, 14	X
UT-SCC-54B	9.3	17	14, 18	31, 32.2	8, 9	12, OL	14	11	20, 24	11, 12	10	12	21, 26	16	10, 14	X
UT-SCC-54C	8, 9	12, 19	16, 22	29, 30	8	11, 12	12, 13	10, 11	16	11, 13	7, 11	11, 12	18, 23	16, 17	12, 14	X
UT-SCC-59C	7, 8, 9.3	15, 17, 18	(14), 17, 18	30, 30.2, (31, 32.2)	8, (9), 11	12	14, 15	11, 12	(24), 25	(11, 12), 13	10, 11, 12	9, 11, 12	(21), 23, 26	16, 18	10, 11, 14	XY
UT-SCC-60A	8, 9	16	18, 19	30.2	8	9, 10	13, 16	12	17, 25	9, 12	11	11, 12	20, 21	12, 16	9, 13	X
UT-SCC-63A	9, 9.3	16	15, 17	31, 31.2	8	7	12, 15	11, 12	20	13	11, 12	9, 11	24	15	13, 14	X
UT-SCC-74A	8	15, 16	14, 17	27	8	10	15, 16	11, 12	18, 19	11, 12	10, 13	12, 14	27	16	10, 12	X(Y)
UT-SCC-74B	8	(12), 16, (17)	14, 17	27	8	10, (11)	(12), (13), 15	11, 12	18, 19	12	10, 13	12, 14	24	16	10, (11), 12	X
UT-SCC-76A	6, 7	15	17, 18	33.2	8, 11	8, 10	15, 16	11	20, 25	11, 12	13	12, 13	22	15	(14), 15	X
UT-SCC-76B	6, 9.3	17	17, 18	28, 30	8, 11	8, 11	13	11, 12	19, 24	9, 12	11, 12	13	24	19	10, 13	XY
UT-SCC-110A	8	14, 17	16, 17	31, 31.2	8, 10	9, 12	14, 16	11	20	11, 12	10, 11	8	20	13, 16, 17	11, 14	X
UT-SCC-110B	8	14, 17	16, 17	30, 31.2	8, 10, (11)	9, 12	14, 16	11, (12)	20, 26	11, 12	10, 11	8, 13	20, 21	16, 17	11, 14	X
UT-SCC-126A	8, 9	16	17, 18	28, 30	9, 11	10	14, 15	11, 12	19	12, 13	10, 13	9, 12	22	13	13, 14	X

Table S4. Composition of cell culture media. Fetal bovine serum (FBS) was acquired from Moregate Biotech (Queensland, Australia). All other reagents were procured from Thermo Fisher Scientific (Waltham, MA).

Cell line(s)	Base medium	Additives
SCC-4	DMEM–HAM'S F12	10% FBS 400 ng.ml^{-1} hydrocortisone Penicillin/streptomycin
SCC-9	DMEM–HAM'S F12	10% FBS 400 ng/ml hydrocortisone 2 mM glutamine 0.5 mM sodium pyruvate Penicillin/streptomycin
FaDu	MEM-alpha	10% FBS Penicillin/streptomycin
SCC-7	DMEM	10% FBS 2 mM L-glutamine
UT-SCC series	MEM	10% FBS 4.5 mg.mL^{-1} D-glucose 1.9 mg.mL^{-1} sodium bicarbonate 1 mM sodium pyruvate 20 mM HEPES Penicillin/streptomycin

Table S5. Cell seeding densities for IC_{50} assay in 96-well microtiter plates. Seeding numbers for each cell line were determined to be within the linear dynamic assay range by titrating seeding density and assessing sulphorhodamine B colorimetry after 5 d in culture.

Cell line(s)	Cells seeded per well
UT-SCC-42B	600
UT-SCC-60A, UT-SCC-74B	800
UT-SCC-74A	1000
UT-SCC-110A, UT-SCC-24A	1200
SCC-4, SCC-9, FaDu	1500
UT-SCC-54B, UT-SCC-63A, UT-SCC-76A, UT-SCC-59C	2000
UT-SCC-42A	2200
UT-SCC-110B, UT-SCC-16A, UT-SCC-46A	2500
UT-SCC-126A	3000
UT-SCC-19A, UT-SCC-54A	3500
UT-SCC-1A	4000
UT-SCC-79A	5000

4. Histology and clinical history of patient-derived xenograft models

4.1 ACS-HN06 Clinical

T4a N2b M0 p16 negative squamous cell carcinoma of the oropharynx, centred on the right base of the tongue. The primary tumor at the tongue base was large and ulcerating, approximately 38 mm, crossing midline, extending onto the soft palate, involving retromolar trigone and pterygoids. Pre-surgical radical chemo-radiotherapy completed: 70 Gy in 35 fractions over 7 weeks, with concurrent high-dose cisplatin (100 $mg.m^{-2}$) given in weeks 1, 4 and 7. At the time of resection (recurrence post chemo-radiotherapy), a 35-mm tumor extended into soft palate and parapharyngeal space. Right mental nerve deficit, right greater palatine nerve intact. No cervical lymphadenopathy. At the time of resection, positive for lymphovascular invasion and perineural invasion (2/19 nodes positive in level 2). Sections showed a 5 × 2 mm sample of moderately differentiated squamous cell carcinoma infiltrating muscle. There was a light peri-tumor neutrophilic infiltrate. There was no significant vascularity within the tumor and there was no lymphovascular space invasion in this sample. The mitotic count was 2 per 10 high power fields.

4.2 ACS-HN06 PDX

Sections showed a 7 × 6 mm sample with a moderately-differentiated squamous cell carcinoma infiltrating fatty tissue. There was a light peri-tumor neutrophilic infiltrate, similar to the clinical ACS-HN06 specimen. There was no significant vascularity within the tumor and there was no lymphovascular space invasion in this sample. The mitotic count was 39 per 10 high power fields.

4.3 ACS-HN07 Clinical

Initially: T4a N0 M0 squamous cell carcinoma of the right inferior alveolus. Recurrence: T3 N0 M0 squamous cell carcinoma (second primary) of the right anterior floor of the mouth and lateral oral tongue. First primary: a large tumor (40 mm in maximum extent) in the right floor of the mouth involving the alveolus and extending into the gingivolabial sulcus. Recurrence: large ulcerated lesion (30 mm well-differentiated squamous cell carcinoma) affecting the right lateral oral tongue, extending onto the neo-floor-of-mouth free flap reconstruction. Initially: early involvement of the mental nerve (hyperesthesia), but no perineural invasion or lymphovascular invasion. Recurrence: positive for lymphovascular and perineural invasion, but no positive neck nodes. Sections showed a 3 × 2 mm sample with a well-differentiated squamous cell carcinoma infiltrating fibromuscular tissue. There was a light lymphoplasmacytic inflammatory infiltrate associated with the tumor. There was no significant vascularity within the tumor and there was no lymphovascular space invasion in this sample. The mitotic count was 11 per 10 high power fields.

4.4 ACS-HN07 PDX

Sections showed three pieces of tissue collectively 10 × 8 mm. These showed fatty tissue infiltrated by a well-differentiated squamous cell carcinoma. There was a moderately dense neutrophilic rather than lymphoplasmacytic inflammatory infiltrate. The neutrophils were reacting to the keratin produced by the tumor. There was no significant vascularity within the tumor and there was no lymphovascular space invasion in this sample. The mitotic count was 8 per 10 high power fields.

4.5 ACS-HN08 Clinical

T4a N2b M0 squamous cell carcinoma of the left oral tongue; 7 cm lesion on the left posterior oral tongue, extending into the angio-oral tongue and the left tongue base up to the soft palate. Sections showed a 6 × 3 mm tissue with a moderately-differentiated squamous cell carcinoma infiltrating fibromuscular tissue. This was associated with a moderately dense inflammatory infiltrate composed of a mixture of neutrophils, plasma cells and lymphocytes. There was no significant vascularity within the tumor and there was no lymphovascular space invasion in this sample. The mitotic count was 26 per 10 high power fields.

4.6 ACS-HN08 PDX

Sections showed a 5 × 4 mm tissue with a moderately-differentiated squamous cell carcinoma. The entire sample was represented by this sheet of tumor, in which case, assessment of the extent of peri-tumor inflammatory response was not possible. There was no significant vascularity within the tumor and there was no lymphovascular space invasion in this sample. The mitotic count was 26 per 10 high power fields.

5. References

1. Nagalla S et al. Interactions between immunity, proliferation and molecular subtype in breast cancer prognosis. *Genome Biol.* 2013;14(4):R34.

2. Toustrup K et al. Development of a hypoxia gene expression classifier with predictive impact for hypoxic modification of radiotherapy in head and neck cancer. *Cancer Res.* 2011;71(17):5923–5931.

3. Sanjana NE, Shalem O, Zhang F. Improved vectors and genome-wide libraries for CRISPR screening. *Nat. Methods* 2014;11(8):783–784.

4. Shalem O et al. Genome-scale CRISPR-Cas9 knockout screening in human cells. *Science (80-.).* 2014;343:84–88.

5. Luo B et al. Highly parallel identification of essential genes in cancer cells. *Proc. Natl. Acad. Sci. U. S. A.* 2008;105(51):20380–5.

6. Mi H et al. PANTHER version 11: Expanded annotation data from Gene Ontology and Reactome pathways, and data analysis tool enhancements. *Nucleic Acids Res.* 2017;45(D1):D183–D189.

7. Araki H, Knapp C, Tsai P, Print C. GeneSetDB: A comprehensive meta-database, statistical and visualisation framework for gene set analysis. *FEBS Open Bio* 2012;2:76–82.

8. Li W et al. MAGeCK enables robust identification of essential genes from genome-scale CRISPR/Cas9 knockout screens. *Genome Biol.* 2014;15(12):554.

9. Doench JG et al. Optimized sgRNA design to maximize activity and minimize off-target effects of CRISPR-Cas9.. *Nat. Biotechnol.* 2016;34(2):184–91.

10. Smurnyy Y et al. DNA sequencing and CRISPR-Cas9 gene editing for target validation in mammalian cells. *Nat. Chem. Biol.* 2014;10(8):623–625.

11. Itoh G et al. CAMP (C13orf8, ZNF828) is a novel regulator of kinetochore-microtubule attachment. *EMBO J.* 2011;30(1):130–144.